Astrophysical Line Diagnosis Requires Nonlinear Dynamical Atomic Modeling

Natalia S. Oreshkina, Stefano M. Cavaletto, Christoph H. Keitel, and Zoltán Harman
Max-Planck-Institut für Kernphysik, Saupfercheckweg 1, 69117 Heidelberg, Germany
(Received 3 July 2014; revised manuscript received 19 August 2014; published 29 September 2014)

Line intensities and oscillator strengths for the controversial $3C$ and $3D$ astrophysically relevant lines in neonlike Fe^{16+} ions are calculated. A large-scale configuration-interaction calculation of oscillator strengths is performed with the inclusion of higher-order electron-correlation effects, suggesting that these contributions cannot explain existing discrepancies between theory and experiment. Then, we investigate nonlinear dynamical effects, showing that, for strong x-ray sources, the modeling of the spectral lines by a peak with an area proportional to the oscillator strength is not sufficient. The dynamical effects give a possible resolution of discrepancies of theory and experiment found by recent measurements, which motivates the use of light-matter interaction models also valid for strong light fields in the analysis and interpretation of astrophysical and laboratory spectra.

DOI: 10.1103/PhysRevLett.113.143001 PACS numbers: 31.15.am, 32.30.Rj, 32.70.-n, 95.85.Nv

Astrophysical spectra recorded by space observatories provide the only means to determine the element composition, temperature, density, and velocity of distant celestial objects such as stars, x-ray binaries, black-hole accretion disks, or active galactic nuclei [1–9]. Such x-ray (or optical) spectra are often composed of a series of peaks associated with a range of elements, ionic charge states, and transitions. Therefore, a large amount of reliable atomic data is needed to disentangle the physical properties of the emitting objects. Such data—transition energies and probabilities, oscillator strengths, collisional and recombination cross sections, etc.—may be obtained from laboratory experiments (see, e.g., [3,10–16]) or, more economically, from theoretical calculations (e.g., [17–20]).

The x-ray emission lines of highly charged Fe ions, in particular Fe^{16+}, are among the brightest in astrophysical spectra [6]. Within the last decade, several observations were performed with the orbiting laboratories Chandra and XMM-Newton (see, e.g., [5,6,21,22]). The x-ray spectrum of Fe^{16+} is, however, not properly reproduced by astrophysical models. The line-strength ratio of two $2p \rightarrow 3d$ lines in Fe^{16+}, customarily denoted as $3C$ and $3D$ [23], was observed, but astrophysical results for the $3C/3D$ ratio are lower than predicted values [4,5], influencing the analysis of space observatory data [6]. Laboratory measurements using an electron beam to excite the Fe ions yielded electron-impact-excitation cross sections which disagree with calculations [7,24], hinting towards an incompleteness in atomic structure or collision theory. The possible sources of astrophysical discrepancy have been further narrowed down after the very first laser spectroscopic experiment in the x-ray regime [3], enabled by the advent of x-ray free-electron-laser (XFEL) facilities [25]. This experiment, employing a purely photonic excitation of the ions, gave hints for a shortcoming of atomic structure theory: a disagreement between all theoretical predictions (ratio of the $3C$ and $3D$ oscillator strengths around 3.5 and above) and the experimental line-strength ratio of 2.61(23) has been stated [3]. In the comparison, as in previous astrophysical modeling, it was assumed that the intensity of a line is proportional to the electric dipole oscillator strength.

In this Letter, motivated by the above discrepancy, we refine the theory of x-ray-ion interactions by calculating higher-order electron-correlation and dynamical effects contributing to the $3C/3D$ line-strength ratio. Our results suggest that the disagreement with the recent laboratory experiment [3] may be removed by the inclusion of nonlinear dynamical effects present in the case of strong driving fields. The broadening of the spectral lines due to the high x-ray intensity depends on the large dipole momenta of the transitions involved, significantly influencing both the line strengths as well as their ratio.

Higher-order correlation and quantum electrodynamical corrections to the oscillator strengths.—To improve the atomic structure theory of the dipole transition rates, we first apply a large-scale implementation of the configuration-interaction Dirac-Fock-Sturm (CI-DFS) method [26,27], which uses radial wave functions obtained by the numerical solution of the Dirac-Fock equation for the occupied orbitals ($1s$, $2s$, $2p$, $3d$), and virtual orbitals with positive and negative energies represented by a relativistic Sturmian basis set. These orbitals are employed to construct configuration state functions, i.e., Slater determinants $|\Phi_J^i\rangle$ ($i = 1, \ldots, N$, where N is the total number of configurations) in an angular momentum-coupled basis with a total angular momentum J. The atomic wave function $|\Psi_J\rangle$ is finally represented as a linear combination of a large set of configurations: $|\Psi_J\rangle = \sum_{i=1}^{N} c_i |\Phi_J^i\rangle$. The Einstein coefficients A_{eg} and oscillator strengths f_{eg} are calculated with such wave functions representing the $2p^6$ ground (g) and excited $[e \in \{(2p^5)_{1/2}3d_{3/2}, (2p^5)_{3/2}3d_{5/2}\}]$ states [28]

$$A_{eg} = \frac{4\pi^2 e^2 c^2}{g_g \omega_{eg}} \sum_{M_e, M_g} \sum_{\vec{k}/k, \sigma} |\langle e|\vec{\alpha}\vec{\epsilon}_{\vec{k}\sigma} e^{-i\vec{k}\vec{r}}|g\rangle|^2,$$

$$f_{eg} = \frac{g_e}{g_g} \frac{A_{eg} m c^3}{2\omega_{eg}^2 e^2}. \quad (1)$$

Here, g_g (g_e) is the degeneracy of the ground (excited) state, the summation goes over the magnetic quantum numbers of the initial and final states and the polarization σ of the emitted photon, and, in addition, an integration is performed over the direction $\vec{k}/k$ of the emitted photon. The constants c, e, and m have their usual meaning, and $\vec{\alpha}$ and $\vec{\epsilon}_{\vec{k}\sigma}$ stand for the vector of alpha matrices and the photon polarization unit vector. The dimensionless oscillator strength is of particular interest, because for low driving-field intensities it is proportional to the line strength, here given as the integrated peak area of the resonance photon scattering cross section [28,29]

$$S_{eg} = \frac{\pi^2 c^2 \hbar^3}{(\hbar\omega_{eg})^2} \frac{g_e}{g_g} A_{eg} \propto f_{eg}. \quad (2)$$

In order to match the accuracy of the experimental transition energies $\omega_{eg} = \omega_e - \omega_g$, additional quantum-electrodynamic (QED) corrections are taken into account in an *ab initio* manner. The QED corrections in first order in the fine-structure constant consist of the self-energy (SE) and vacuum-polarization terms. The SE correction is decomposed into zero-, one-, and many-potential terms. The zero-potential and one-potential terms are calculated in momentum space using formulas from Ref. [30]. The residual part of the SE correction, the so-called many-potential term, is calculated in coordinate space. For any given intermediate-state angular momenta, the summation over the Dirac spectrum is performed using the dual-kinetic-balance approach [31] with basis functions constructed from B splines. The vacuum-polarization correction was calculated in the Uehling approximation [32]. Electron-interaction contributions to the QED corrections were calculated by evaluating the single-electron QED diagrams with an effective potential accounting for the screening of the remaining nine electrons (see [14]). We find that, although screening effects significantly modify the single-electron QED corrections, the total QED effect on the transition energies is on the 10-meV level.

While we can conclude that transition energies entering the theoretical oscillator strengths can be predicted with sufficient accuracy, the discrepancy with the measurements prevails and it may be rooted in the calculation of the nondiagonal dipole matrix elements. In previous theoretical studies, it was assumed that the many-electron wave function can be well represented by constructing the configuration space with single and double exchanges from the reference-state configuration. Here, we also take into account triple excitations, resulting in a huge number of configurations. As a result, for the case of single and double excitations included, the $3C/3D$ oscillator strength ratio is 3.57, while the contribution of the triple excitation is as low as -0.01. Thus, our results confirm earlier theoretical calculations and disprove the significance of triple excitations, suggesting that the discrepancy of theory and experiment is not funded in the inaccurate description of the ions' electronic structure.

Modeling of strong-field effects.—Once insufficiencies in structure calculations are ruled out, the next to be investigated are dynamical aspects of light-matter interaction. In Ref. [3] and in previous studies, it was implicitly assumed that the intensity of the observed lines is proportional to the oscillator strength. This holds true under the assumption of a relatively weak exciting field. However, nonlinearities are anticipated if the intensity I of the field is comparable to or larger than the saturation intensity I_{sat}, to be defined below. For the Fe transitions studied, the large dipole-moment matrix element leads to $I_{\mathrm{sat}} \approx 10^{11}$ W/cm^2, and, since the intensity of Linac Coherent Light Source (LCLS) pulses is typically on or above this order of magnitude, the exciting field cannot be considered as weak anymore.

We, therefore, improve the physical description and perform time-dependent simulations by modeling the ion as a two-level system with ground state $|g\rangle$ and excited state $|e\rangle$. The transition energy ω_{eg} approximately equals 826 eV and 812 eV for the $3C$ and $3D$ lines, respectively, and the decay width is $\Gamma_{eg} = \hbar A_{eg}$. We describe the atomic system via the density matrix $\hat{\rho}(t)$ of elements ρ_{ij}, with $i, j \in \{g, e\}$, whose evolution in time is given by the master equation [33,34]

$$\dot{\hat{\rho}} = -\frac{i}{\hbar}[\hat{H}, \hat{\rho}(t)] + L\hat{\rho}(t), \quad (3)$$

where the square brackets stand for a commutator, and the Lindblad superoperator L represents the spontaneous decay from the exited state $|e\rangle$ to the ground state $|g\rangle$ with decay rates equal to 2.22×10^{13} s^{-1} and 6.02×10^{12} s^{-1} for the $3C$ and the $3D$ transitions, respectively, according to our CI-DFS calculations. The Hamiltonian $\hat{H} = \hat{H}_0 + \hat{H}_{\mathrm{int}}$ is the sum of the electronic-structure Hamiltonian $\hat{H}_0 = \sum_{i\in\{g,e\}} \hbar\omega_i |i\rangle\langle i|$ and of the Hamiltonian $\hat{H}_{\mathrm{int}}$ describing the interaction of the ion with an external time-dependent electric field $\mathcal{E}(t) = E(t)\cos[\omega_{\mathrm{X}} t + \psi(t)]$ of x-ray carrier frequency ω_{X}, envelope $E(t)$, and phase $\psi(t)$. We introduce the vector $\vec{R}(t)$ of the slowly varying components of the density matrix,

$$\vec{R}(t) = (\rho_{gg}(t), \rho_{ge}(t)e^{-i\omega_{\mathrm{X}} t}, \rho_{eg}(t)e^{i\omega_{\mathrm{X}} t}, \rho_{ee}(t))^{\mathrm{T}}, \quad (4)$$

such that Eq. (3) can be written in the matrix form

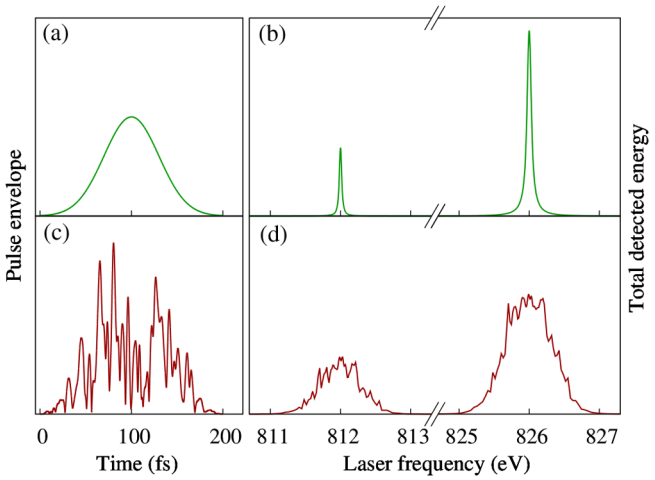

FIG. 1 (color online). (a) Time envelope of a Gaussian and (c) an incoherent pulse, in arbitrary units. (b), (d) The fluorescence signal (total energy of fluorescence photons) as a function of the XFEL photon energy in the energy range of the $3C$ and $3D$ transitions in Fe^{16+}, in arbitrary units. Here, an x-ray intensity of $I = 10^{13}$ W/cm^2 was used and results are shown for (c) a Gaussian pulse and (d) after averaging over 10 incoherent pulses with a time duration of $T = 200$ fs. For incoherent pulses, the bandwidth is set to $B = 1$ eV.

$$\dot{\vec{R}}(t) = \mathbf{M}(t)\vec{R}(t), \tag{5}$$

with the 4×4 time-dependent matrix

$$\mathbf{M}(t) = \begin{pmatrix} 0 & -i\frac{\Omega_R^*(t)}{2} & i\frac{\Omega_R(t)}{2} & \Gamma_{eg} \\ -i\frac{\Omega_R(t)}{2} & i\Delta - \frac{\Gamma_{eg}}{2} & 0 & i\frac{\Omega_R(t)}{2} \\ i\frac{\Omega_R^*(t)}{2} & 0 & -i\Delta - \frac{\Gamma_{eg}}{2} & -i\frac{\Omega_R^*(t)}{2} \\ 0 & i\frac{\Omega_R^*(t)}{2} & -i\frac{\Omega_R(t)}{2} & -\Gamma_{eg} \end{pmatrix}.$$

The complex time-dependent Rabi frequency $\Omega_R(t) = eE(t)\langle g|\hat{r}|e\rangle e^{i\psi(t)}/\hbar$ is proportional to the square root of the x-ray intensity I and $\Delta = \omega_{eg} - \omega_X$ denotes the detuning of the laser frequency from the transition frequency. For a continuous-wave driving field, $E(t) = \bar{E}$, $\psi(t) = 0$, with correspondingly constant Rabi frequency $\bar{\Omega}_R$, the solution of the master equation (5) converges for $t \to \infty$ to the stationary solution [29,33]

$$\bar{R}_{ee}(\Delta) = \frac{\bar{\Omega}_R^2}{4\Delta^2 + \Gamma_{eg}^2 + 2\bar{\Omega}_R^2}. \tag{6}$$

The energy detected per unit time for given detuning is $\mathcal{I}(\Delta) \propto \Gamma_{eg}\omega_{eg}\bar{R}_{ee}(\Delta)$, which can be used to calculate the ratio of the intensities emitted by the two lines by means of the integrals over the detuning Δ

$$S_{3C}/S_{3D} = \int d\Delta \mathcal{I}_{3C}(\Delta) \Big/ \int d\Delta \mathcal{I}_{3D}(\Delta). \tag{7}$$

By introducing, for each line, the saturation intensity $I_{\text{sat}} = I\Gamma_{eg}^2/(2\bar{\Omega}_R^2)$, this leads to

$$S_{3C}/S_{3D} = \frac{\Gamma_{3C}\omega_{3D}^2}{\Gamma_{3D}\omega_{3C}^2}\sqrt{\frac{1 + I/I_{\text{sat},3D}}{1 + I/I_{\text{sat},3C}}}. \tag{8}$$

For a weak exciting field ($I \ll I_{\text{sat}}$), this agrees with the linear theory of resonance fluorescence predicting a ratio of 3.56, while in the strong-field limit ($I \gg I_{\text{sat}}$), Eq. (8) converges to the value $S_{3C}/S_{3D} \to 7.03$.

For a time-dependent (pulsed) driving field, the system of differential equations (5) is solved assuming the initial conditions $\vec{R}_0 = (1, 0, 0, 0)^T$. Thereby, we can calculate the total detected energy as a function of the detuning

$$\mathcal{E}(\Delta) \propto \Gamma_R\omega_{eg}\int_{-\infty}^{+\infty} R_{ee}(t)dt, \tag{9}$$

where $R_{ee}(t)$ also depends on Δ. This yields a spectrum which can be compared to the experimentally measured one. The ratio of total emitted line energies can, again, be calculated as a ratio of the integrals over the detuning Δ

$$S_{3C}/S_{3D} = \int d\Delta \mathcal{E}_{3C}(\Delta) \Big/ \int d\Delta \mathcal{E}_{3D}(\Delta). \tag{10}$$

In the experiment [3], the LCLS provided x-ray bunches with up to 3 mJ total energy per shot. Although the pulse parameters are not well known and are not fixed from pulse to pulse because of their chaotic nature and loss in the monochromator used, assuming a photon beam diameter between 0.1 and 1 mm and pulse durations between 200 and 2000 fs, the intensities can be estimated to be in the range of $I = 10^{11}$–10^{14} W/cm^2. Also, not the total energy emitted in all directions was detected in the experiment [3], but only a fraction of it emitted into a given solid angle. However, since the excited states have the same symmetry (total angular momentum $J = 1$) and the ground state of the ion is spherically symmetric ($J = 0$), the angular distribution of the emitted radiation is the same for both transitions, allowing one to compare the strength ratio as defined above with the experimentally determined line intensities.

Matching the experimental line strengths and discussion.—In Fig. 1(b), simulated $3C$ and $3D$ fluorescence lines are presented assuming strong XFEL pulses of Gaussian shape for an intensity of $I = 10^{13}$ W/cm^2 and duration of $T = 200$ fs. We use the pulse envelope $E(t) = E_{\max}e^{-(t^2/T^2)32\ln(2)}$ and a constant phase $\psi(t) = 0$. The ratio of the $3C$ and $3D$ line strengths is shown separately in Fig. 2 as a function of the pulse parameters. The strengths and their ratio are sensitive to the change of pulse intensity

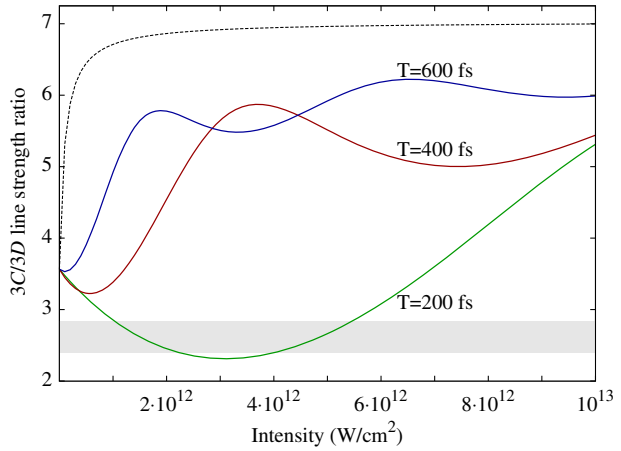

FIG. 2 (color online). The line-strength ratio S_{3C}/S_{3D} as a function of the intensity and duration of the Gaussian pulse. The dashed line is for a continuous wave field [Eq. (7)]. The gray shaded area shows the experimental ratio 2.61(23) [3] together with its error bar.

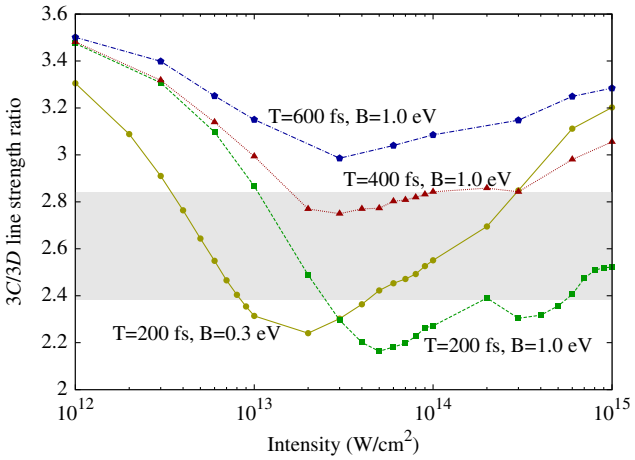

FIG. 3 (color online). The line-strength ratio S_{3C}/S_{3D} as a function of the intensity I and duration T of the incoherent pulse. For the shortest pulses, results with two different bandwidths B are shown. The gray shaded area shows the experimental ratio 2.61(23) [3] together with its error bar.

and duration. Between $I = 1 - 6 \times 10^{12}$ W/cm^2 and for $T = 200$ fs, the resulting line-strength ratio is in the range of 2.31–3.08, as presented in Fig. 2. This result is still in agreement with the measured value of 2.61 ± 0.23. We also infer that the pulse-by-pulse variation of intensity and duration contributes to the experimental uncertainty of the ratio. These results confirm the importance of strong-field dynamical effects in a relatively intense XFEL field. We note that, in this range of parameters, we are still in the weakly nonlinear regime: below intensities of approximately 10^{11} W/cm^2, the linear theory of resonance fluorescence may be applied. (The linear model is also applicable for transitions with significantly lower dipole matrix elements, even if the intensity of the x-ray source is high.) At higher intensities, or for longer pulses, which is also still in the range of possible experimental parameters, the sensitivity to the pulse parameters increases, resulting in an oscillation of the line-strength ratio of the $3C$ and $3D$ lines between 5.5 and 6.5, in agreement with the previously mentioned intensity-saturation effects. Increasing the pulse duration in the simulations, one reaches the limit of continuous-wave fields, which is shown by the dashed line [cf. Eq. (7)].

For an even more realistic modeling, we, additionally, take into account the chaotic nature of XFEL pulses generated via self-amplified spontaneous emission [35], by modeling amplitude $E(t)$ and phase $\psi(t)$ via the partial-coherence method [36,37]. An understanding of incoherence effects is not only relevant for laboratory measurements, but also for astrophysical observations, as natural x-ray sources lack coherence. In the simulations, we employ a series of randomized pulses, an example of which is shown in Fig. 1(c). Figure 1(d) presents the fluorescence signal resulting from the use of such incoherent pulses, while Fig. 3 displays the line-strength ratio (10) obtained with chaotic pulses of different duration, intensity, and bandwidth. Each point in Fig. 3 is obtained by averaging over 10 independent realizations of a chaotic pulse. The numerical uncertainty of the obtained results is estimated to be ~1%–2%. As in the case of Gaussian pulses, the line-strength ratio clearly depends on the pulse parameters. Also here, for low intensities, the value of 3.56 is approached, in agreement with the linear theory of resonance fluorescence. We notice that, for incoherent pulses, a decrease in the $3C/3D$ line-strength ratio can be observed within a wider range of pulse intensities than for Gaussian pulses, as well as for a significantly larger interval of pulse durations. As shown in the picture, this effect becomes more significant at increasing values of the bandwidth (i.e., the FWHM of the energy spectrum) of the chaotic pulse, which, in the experiment [3], can be estimated to be ~1 eV. The decrease in bandwidth (increase in coherence time) corresponds to a more coherent pulse, and a behavior closer to that displayed by fully coherent (transform-limited) Gaussian pulses.

As estimated before, intensities in [3] were in the range of $I = 10^{11}$–10^{14} W/cm^2. Most pulses had durations corresponding to those of the curves in Fig. 2 and Fig. 3. The use of a monochromator in [3] causes a decrease in pulse peak intensities; we notice, however, that the decrease in bandwidth B is shown in Fig. 3 to require lower pulse intensities to obtain the same $3C/3D$ line strength ratio. The predicted decrease in the $3C/3D$ ratio within a broad interval of pulse intensities and durations suggests that the observed unexpectedly low laboratory value of the $3C/3D$ ratio is determined by previously neglected nonlinear dynamical effects, thus, depending on the precise XFEL parameters, either resolving or decreasing the discrepancy of state-of-the-art atomic structure theories with the XFEL measurement [3]. This implies for astrophysical studies that weak-field atomic theory employing the best structure models is applicable for

astrophysical sources of low intensities, while previously neglected strong-field dynamical effects have to be included for sources in the regime of the saturation intensity or above.

In summary, we have demonstrated that higher-order electron-correlation effects, considered so far [3] as the most likely source of the discrepancy of atomic theory with recent laboratory measurements, only marginally influence the oscillator strengths of the $3C$ and $3D$ lines in Fe^{16+} ions. The same holds for QED corrections. Instead, considering intensity-dependent nonlinear effects, neglected so far, was shown to be crucial. For accurately incorporating those modifications, an improved experimental determination of the XFEL parameters is called for because, for certain realistic parameters within the possible range, here we could explain the discrepancy [3] via those dynamical effects. Approaching the saturation intensity, the weak-field atomic theory employed so far is shown not to be applicable anymore, which is equally valid for corresponding astrophysical scenarios. For instance, in the accretion disk of stellar-mass black holes in x-ray binaries [38], the Eddington luminosity of $\sim 10^{38}$ erg/s at a distance close to the innermost stable orbit of three Schwarzschild radii leads to an intensity of approximately 3×10^{13} W/cm^2 for a line at 1 keV with a 1-eV width, requiring the inclusion of the previously neglected nonlinear dynamics.

We acknowledge helpful advice from Ilya I. Tupitsyn and insightful conversations with Alberto Benedetti.

[1] M. Díaz Trigo, J. C. A. Miller-Jones, S. Migliari, J. W. Broderick, and T. Tzioumis, Nature (London) **504**, 260 (2013).

[2] J.-F. Liu, J. N. Bregman, Y. Bai, S. Justham, and P. Crowther, Nature (London) **503**, 500 (2013).

[3] S. Bernitt, G. V. Brown, J. K. Rudolph, R. Steinbrügge, A. Graf, M. Leutenegger, S. W. Epp, S. Eberle, K. Kubiček, V. Mäckel *et al.*, Nature (London) **492**, 225 (2012).

[4] E. Behar, J. Cottam, and S. M. Kahn, Astrophys. J. **548**, 966 (2001).

[5] H. Xu, S. M. Kahn, J. R. Peterson, E. Behar, F. B. S. Paerels, R. F. Mushotzky, J. G. Jernigan, A. C. Brinkman, and K. Makishima, Astrophys. J. **579**, 600 (2002).

[6] F. B. S. Paerels and S. M. Kahn, Annu. Rev. Astron. Astrophys. **41**, 291 (2003).

[7] G. V. Brown, P. Beiersdorfer, H. Chen, M. H. Chen, and K. J. Reed, Astrophys. J. **557**, L75 (2001).

[8] *X-ray Spectroscopy in Astrophysics*, edited by J. van Pradijs and J. A. M. Bleeker (Springer-Verlag, Berlin, 1999).

[9] G. B. Rybicki and A. P. Lightman, *Radiative Processes in Astrophysics* (John Wiley & Sons, New York, 2004).

[10] P. Beiersdorfer, M. Bitter, S. von Goeler, and K. W. Hill, Astrophys. J. **610**, 616 (2004).

[11] P. Beiersdorfer, S. von Goeler, M. Bitter, and D. B. Thorn, Phys. Rev. A **64**, 032705 (2001).

[12] G. V. Brown, P. Beiersdorfer, D. A. Liedahl, K. Widmann, and S. M. Kahn, Astrophys. J. **502**, 1015 (1998).

[13] M. Hahn, N. R. Badnell, M. Grieser, C. Krantz, M. Lestinsky, A. Müller, O. Novotný, R. Repnow, S. Schippers, A. Wolf *et al.*, Astrophys. J. **788**, 46 (2014).

[14] K. Schnorr, V. Mäckel, N. S. Oreshkina, S. Augustin, F. Brunner, Z. Harman, C. H. Keitel, J. Ullrich, and J. R. Crespo López-Urrutia, Astrophys. J. **776**, 121 (2013).

[15] J. K. Rudolph, S. Bernitt, S. W. Epp, R. Steinbrügge, C. Beilmann, G. V. Brown, S. Eberle, A. Graf, Z. Harman, N. Hell *et al.*, Phys. Rev. Lett. **111**, 103002 (2013).

[16] E. W. Schmidt, D. Bernhardt, A. Müller, S. Schippers, S. Fritzsche, J. Hoffmann, A. S. Jaroshevich, C. Krantz, M. Lestinsky, D. A. Orlov *et al.*, Phys. Rev. A **76**, 032717 (2007).

[17] A. K. Bhatia and G. A. Doschek, At. Data Nucl. Data Tables **52**, 1 (1992).

[18] M. Cornille, J. Dubau, and S. Jacquemot, At. Data Nucl. Data Tables **58**, 1 (1994).

[19] U. I. Safronova, C. Namba, I. Murakami, W. R. Johnson, and M. S. Safronova, Phys. Rev. A **64**, 012507 (2001).

[20] G. X. Chen, Phys. Rev. A **76**, 062708 (2007).

[21] D. P. Huenemoerder, A. Mitschang, D. Dewey, M. A. Nowak, N. S. Schulz, J. S. Nichols, J. E. Davis, J. C. Houck, H. L. Marshall, M. S. Noble *et al.*, Astron. J. **141**, 129 (2011).

[22] R. Mewe, A. J. J. Raassen, J. J. Drake, J. S. Kaastra, R. L. J. van der Meer, and D. Porquet, Astron. Astrophys. **368**, 888 (2001).

[23] $3C$ stands for the $2p^6(J=0) \rightarrow (2p^5)_{1/2}3d_{3/2}(J=1)$ transition at 826 eV and $3D$ for the $2p^6(J=0) \rightarrow (2p^5)_{3/2}3d_{5/2}(J=1)$ transition at 812 eV.

[24] G. V. Brown, P. Beiersdorfer, H. Chen, J. H. Scofield, K. R. Boyce, R. L. Kelley, C. A. Kilbourne, F. S. Porter, M. F. Gu, S. M. Kahn *et al.*, Phys. Rev. Lett. **96**, 253201 (2006).

[25] P. Emma, R. Akre, J. Arthur, R. Bionta, C. Bostedt, J. Bozek, A. Brachmann, P. Bucksbaum, R. Coffee, F.-J. Decker *et al.*, Nat. Photonics **4**, 641 (2010).

[26] I. I. Tupitsyn, V. M. Shabaev, J. R. Crespo López-Urrutia, I. Draganić, R. S. Orts, and J. Ullrich, Phys. Rev. A **68**, 022511 (2003).

[27] I. I. Tupitsyn, A. V. Volotka, D. A. Glazov, V. M. Shabaev, G. Plunien, J. R. Crespo López-Urrutia, A. Lapierre, and J. Ullrich, Phys. Rev. A **72**, 062503 (2005).

[28] I. P. Grant, J. Phys. B **7**, 1458 (1974).

[29] C. J. Foot, *Atomic Physics* (Oxford University Press, New York, 2005).

[30] V. Yerokhin and V. M. Shabaev, Phys. Rev. A **60**, 800 (1999).

[31] V. M. Shabaev, I. I. Tupitsyn, V. A. Yerokhin, G. Plunien, and G. Soff, Phys. Rev. Lett. **93**, 130405 (2004).

[32] E. A. Uehling, Phys. Rev. **48**, 55 (1935).

[33] M. O. Scully and S. Zubairy, *Quantum Optics* (Cambrige University Press, Cambridge, England, 1997).

[34] M. Kiffner, M. Macovei, J. Evers, and C. H. Keitel, Prog. Opt., **55**, 85 (2010).

[35] R. Bonifacio, C. Pellegrini, and L. Narducci, Opt. Commun. **50**, 373 (1984).

[36] T. Pfeifer, Y. Jiang, S. Düsterer, R. Moshammer, and J. Ullrich, Opt. Lett. **35**, 3441 (2010).

[37] S. M. Cavaletto, C. Buth, Z. Harman, E. P. Kanter, S. H. Southworth, L. Young, and C. H. Keitel, Phys. Rev. A **86**, 033402 (2012).

[38] S. L. Shapiro and S. A. Teukolsky, *Black Holes, White Dwarfs and Neutron Stars: The Physics of Compact Objects* (John Wiley & Sons, New York, 1983).